Journal of Alloys and Compounds 766 (2018) 694–704

Contents lists available at ScienceDirect

Journal of Alloys and Compounds

journal homepage: http://www.elsevier.com/locate/jalcom

Local microstructure inhomogeneity and gas temperature effect in *in-situ* shot-peening assisted cold-sprayed Ti-6Al-4V coating

Hongxia Zhou [a, b], Chengxin Li [a, *], Gang Ji [a], Silin Fu [a], Hao Yang [a], Xiaotao Luo [a], Guanjun Yang [a], Changjiu Li [a]

[a] Sate Key Laboratory for Mechanical Behavior of Materials, School of Materials Science and Engineering, Xi'an Jiaotong University, Xi'an, Shaanxi, 710049, China

[b] Qinghai Provincial Key Laboratory of New Light Alloys, Qinghai Provincial Engineering Research Center of High Performance Light Metal Alloys and Forming, Qinghai University, Xining, 810016, China

ARTICLE INFO

Article history:
Received 11 April 2018
Received in revised form
21 June 2018
Accepted 1 July 2018
Available online 2 July 2018

Keywords:
Ti-6Al-4V
Shot peening
Cold spraying
Mechanical property
Microstructure

ABSTRACT

In the cold spraying process, previously deposited particles are hammered by the following particles, and gas temperature plays an important role in coating properties. In this study, By adding large shot peening particles to original Ti-6Al-4V (TC4) powder, five *in-situ* shot peening assisted cold sprayed coatings were obtained using nitrogen accelerating gas at different temperatures, and microstructure and the mechanical properties of coatings were evaluated. No phase transformation occurred during the spraying process, and the deposition efficiency was generally more than 60%. The cross-section morphology showed that the coating became denser with the increase in temperature, and the coating showed a structure of alternating dense and porous regions. Local regions struck by large shot-peening particles were denser than other regions. Therefore, the porosity, microhardness, and elastic modulus were divided into two categories. These two categories showed the same trend with temperature: The porosity decreased, whereas the microhardness and elastic modulus gradually increased. The highest values of the latter two properties were 443.4 $HV_{0.3}$ (tamped region)/390 $HV_{0.3}$ (nontamped region) and 124.8 GPa (tamped region)/110.2 GPa (nontamped region), respectively. Moreover, the bonding and shear strengths increased as the temperature increased, and the fracture morphology showed that brittle fracture was the main type of failure. In addition, by analyzing the microstructure and action depth of shot at different temperatures, it was found that the auxiliary effect of shot peening on the deformation of particles was limited at high gas temperature.

1. Introduction

Ti and its alloys are widely used in the aerospace industry, medical implant, and anticorrosion coatings because of their high special strength, biocompatibility, and corrosion resistance even at high temperatures. The most common alloy Ti-6Al-4V (TC4) features excellent strength, accounting for ~60% of total Ti production [1]. However, owing to the oxygen affinity of Ti and its alloys, they have limited applications in larger areas because of a high production cost due to the requirement of a vacuum environment [2]. Cold gas dynamic spray technology, also known as cold spraying, has the potential to prepare oxidation-sensitive materials.

Cold spraying is an emerging thermal spray technology characterized by a low temperature (almost room temperature) and high speed (up to 1500 m/s); it has been a new member of thermal spray family since its discovery in 1980. To begin with, cold spraying had been used to spray ductile materials such as Cu [3,4], Al [5,6], and Zn [7], but with the development of this technology, nowadays, many refractory metals such as Ti and its alloys [8,9], Ta [10], and superalloys [11], as well as ceramic materials [12] can be fabricated by cold spraying. Cold spraying processes are of interest in the aerospace industry for repair purposes because cold spraying processes overcome the drawbacks such as oxidation and a high thermal stress, which are always encountered in thermal processes such as thermal spray and welding processes [13]. The use of cold spraying is attractive in repair of components, also because of low costs and high productivity of repair processes. Thus, cold spraying is promising for maintenance.

* Corresponding author.
E-mail address: licx@mail.xjtu.edu.cn (C. Li).

https://doi.org/10.1016/j.jallcom.2018.07.009
0925-8388/

In the last few years, many studies on cold-sprayed TC4 showed that the coating exhibited a porous microstructure, and it was difficult to obtain a dense TC4 coating except when using expensive helium as the propellant gas. Up to now, the porosity of cold-sprayed TC4 coatings was reported as 10–25%. This high porosity hindered the improvement of other properties for TC4 coatings. Therefore, one of the problems is how to obtain a dense TC4 cold-sprayed coating using nitrogen as the propellant gas?

Much effort has been devoted to solve this problem. In general, a smaller particle size, more concentrated distribution, and shorter spraying stand-off are beneficial for a denser coating [14,15]. Moreover, extensive studies indicated that a high carrier gas temperature and pressure are beneficial for denser deposits [16–18]. At a given temperature and pressure, preheating the powder softened the particle, increased the particle velocity, and provided a denser structure [19,20]. However, because Ti and its alloys are highly sensitive to oxygen, at a high preheating temperature (>750 °C), oxidation occurs, and a thin oxide film forms on the surface of particle. The results of numerical simulation of Al particles indicate that the oxide film can hinder the deformation of particles and deteriorate the bonding between particles [21]. Furthermore, Huang et al. [22] showed that the optimized nozzle increased the particle velocity and improved the adhesive strength with substrate, as well as decreased the porosity.

In cold-sprayed coating, previously deposited particles are hammered by the following particles, usually leading to an *in-situ* shot-peening effect. In a study on the deposition characteristics of Ti coatings, Li et al. [23] found that the porosity of top layer was much higher than that of bottom layer, and the subsequent particles played a role in deforming the former deposits once again. Based on this phenomenon, it is reasonable that the densification of less plastic metal coatings such as Ti and its alloys can be achieved by adding other hard particles into the spray powder. With the aid of in-situ shot peening of large particles, Ti and its alloys can produce larger deformation. Luo et al. [24] obtained dense Ti and TC4 cold-sprayed coatings using an *in-situ* shot-peening method. The coating hardness increased with increasing the shot-peening particle content and reached to more than 400 HV for TC4 coating. The increase in hardness can be attributed to work hardening and decreased porosity.

In-situ shot peening in cold spraying provides a new way to prepare dense TC4 coatings, but few studies paid attention to the effect of shot reinforcement on the microstructure and mechanical properties of coatings. In this study, we aimed to improve the performance of TC4 cold-sprayed coatings by increasing the propellant gas temperature and adding shot-peening particles, and evaluated local mechanical performance and effect of gas inlet temperature.

2. Experimental

Spherical TC4 gas atomized powder (Raymor Industries Inc., Boisbriand, Canada) was used as the starting powder, and the particle size distribution was measured by the laser diffraction method. The sizes of TC4 particles range from ~15 to ~30 μm with a mean value of ~22.6 μm. Stainless steel 1Cr18 was used as shot-peening particles with a size distribution from ~125 μm to ~300 μm, and the average value was ~181 μm. Both the TC4 and 1Cr18 as-received powders are shown in Fig. 1. As shown in Fig. 1a, the surface of spherical TC4 particles is relatively smooth, and some nano TC4 particles mixed with the initial powders. The particles have a layered structure, and the nanoparticles are present

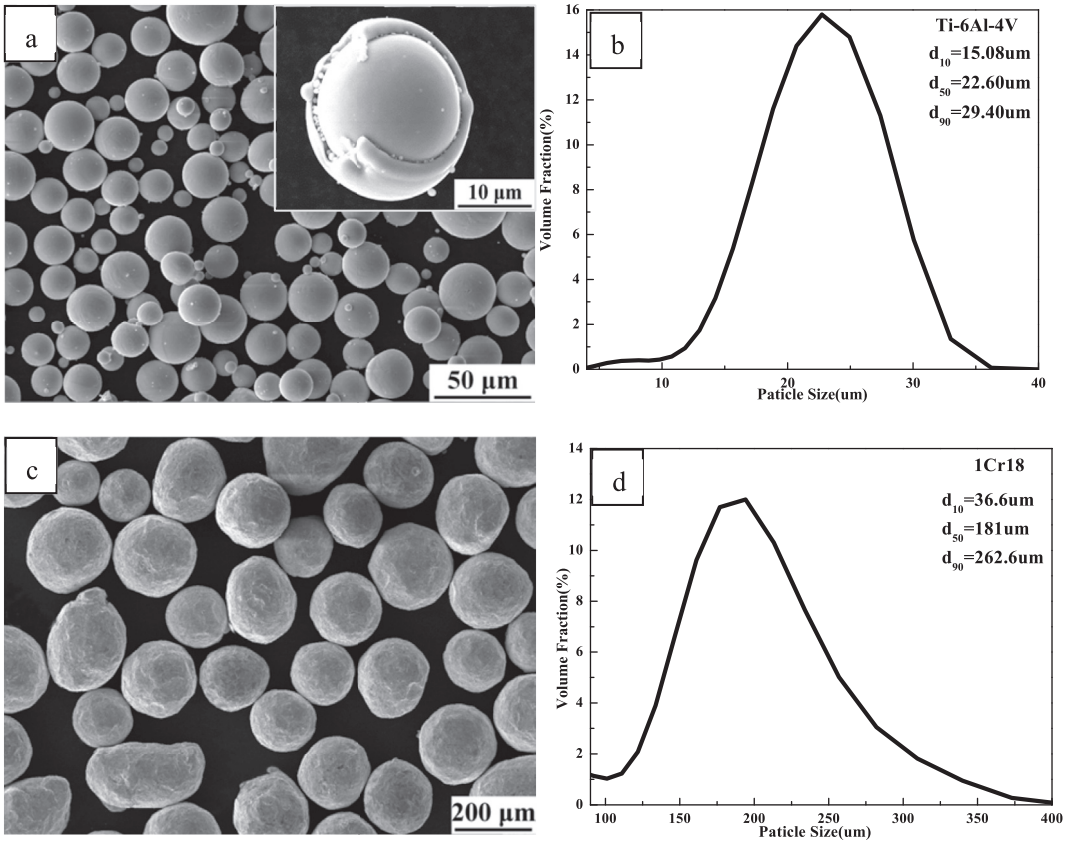

Fig. 1. Morphologies and size distribution of TC4 (a and b) and 1Cr18 shot-peening particles (c and d).

between the layers.

According to our previous study [24], the coating with 70 vol% shot-peening particles achieved the best properties. Therefore, in this study, the content of shot-peening particles was selected as 70 vol%, and they were mixed with TC4 powder by mechanical mixing. The mixture was used as the feedstock for coating deposition. To clarify the effect of gas inlet temperature on the microstructure and mechanical properties of coatings, 550–750 °C with an interval of 50 °C was selected as the accelerating gas temperature. TC4 plates with a thickness of 4 mm were used as the substrate for repairing. Prior to spraying, the substrate was degreased using acetone and grit-blasted with grit alumina to obtain a rough surface.

The coatings were prepared using an in-house cold spraying system, model number CS-2000. In this system, the spray powders are fed along the axis of a convergent–divergent (De-Laval) nozzle with throat and outlet diameters of 2.7 mm and 6 mm, respectively. The length of divergent section was 150 mm. Nitrogen was used as the propellant gas and powder carrier gas; the spraying parameters are shown in Table 1. The coating thickness was >2 mm to satisfy the dimension of shear specimen (The coating thickness used to measure the bonding strength is 300 μm). The substrate with cold-sprayed coating was cut into sizes of 15 mm × 15 mm.

The cross-sections of as-sprayed coatings were prepared by a conventional mechanical polishing method with SiC papers of up to grit #2000 in successively finer grades using an automatic polishing machine, followed by polishing with diamond suspensions. The microstructure of mirror-polished cross-sections was characterized by scanning electron microscopy (SEM).

To analyze the phase transition in coating deposition, a Bruker D8 Advance X-ray microdiffractometer using Cu Kα radiation monochromated with crossed coupled Gobel mirrors operating at 40 keV and 40 mA was used to determine the X-ray diffraction patterns, providing a scan over the 2θ range 20–90° with a step size of 0.02°. Crystalline phases were identified using Jade 6.0 software.

The porosities of specimens were measured from the cross-section of coatings based on image analysis. Ten SEM images were recorded at 1000 × in backscattered electron mode for each sample. The deposition efficiency of coatings was measured by weighing the sample before and after the spraying using an electronic balance (0.1 mg). The microhardness measurement (MICROMET5104, Buehler, Germany) was an average of ten measurements taken at ~0.2 mm from the coating/substrate interface using a 300-g load. The elastic moduli of coatings were estimated from nanoindentation measurements (TI-950 Triboindenter, Hysitron, USA) at 8000 μN load using a technique described elsewhere (Ref. 25). The bonding strength of the coatings was measured using a tensile test machine (Instron 5569) according to the ASTMC633 standard. The top surfaces of cylindrical samples were coated with TC4 coatings and then glued to the respective counterbodies of the same size. The adhesive strength of used glue was 70 MPa. The specimens were tensile tested along their principal axes. The load was applied on the sample until rupture occurred, and the value was recorded. Adhesion tests were performed on five specimens per group for statistical reasons. The shear adhesion strength of specimens was measured using a special fixture attached to an autograph universal testing unit (Instron 5569). A schematic diagram and dimensions of the shear test samples are shown in Fig. 2. The cross-head speed of the shear punch moved at a rate of 0.5 mm/min, and the shear adhesion strength was calculated by dividing the maximum shear pressure with shear area.

3. Results and discussion

3.1. XRD phase analysis

Fig. 3 showed the chemical composition of powder and coatings. The cold spraying technology did not alter the elemental or phase composition of deposited TC4 material. All the coatings were 100% α-Ti; no recognizable peaks for the β phase were observed in the XRD spectrum of coating. Despite the highest gas temperature in this experiment is 750 °C, the temperature of the flying temperature is about 300 °C nearby the critical velocity according to the computer simulations with fluid dynamics simulation approach [25]. Inherent high reactivity of Ti alloy is above 500 °C, but the working gas temperature selected in this experiment did not trigger any reactions with oxygen or nitrogen because of a short dwelling time in the heated gas.

3.2. Microstructure and local mechanical performance

3.2.1. Microstructure

Fig. 4 shows the cross-section morphologies of TC4 coatings deposited at different propelling gas temperatures with the powder comprised of 70 vol% 1Cr18 and 30 vol% TC4. As expected, with the increase in temperature, the coatings became denser. The TC4

Table 1
Spraying parameters of TC4 coatings.

Gas	Gas inlet temperature (°C)	Gas pressure (MPa)	Gun traverse speed (mm/s)	Standoff distance (mm)	Powder feeder rate (g/min)	Spraying angle (°)
N_2	550–750	3	40	20	50	90

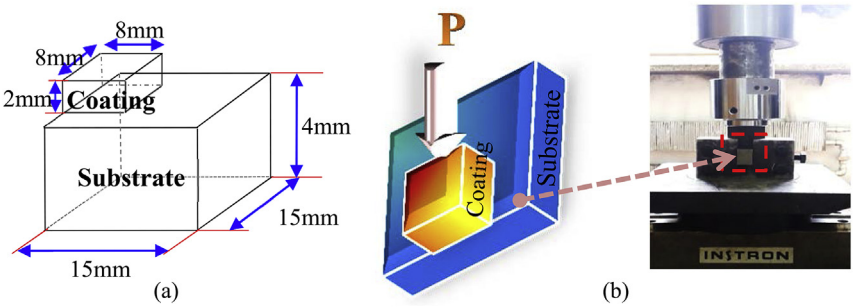

Fig. 2. The dimension(a) and schematic diagram of the shear test (b).

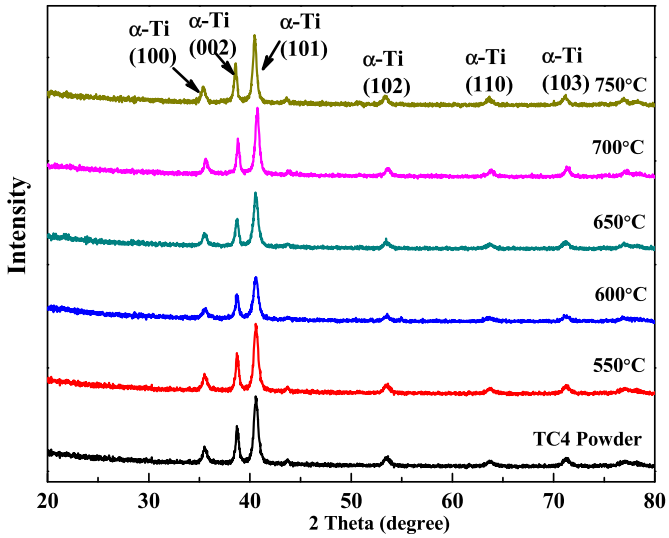

Fig. 3. X-ray diffraction results for the TC4 feedstock powder and coatings.

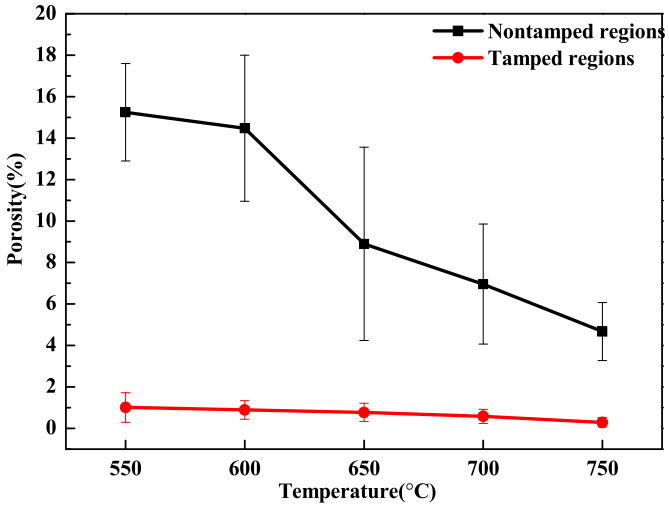

Fig. 5. Porosities of TC4 coatings as a function of the accelerating gas temperature.

coatings deposited at 550 °C and 600 °C have pores throughout its cross-section except the regions nearby the craters left by rebounded shot-peening particles. However, the TC4 coatings deposited at 700 °C and 750 °C have a much smaller number of pores throughout its cross-section compared with those deposited at a low temperature. In five coatings, a clear trace of shot-peening particles was observed, as marked by yellow dotted line. In the coatings prepared at 550 °C and 600 °C, many particles still showed a spherical morphology because of inadequate deformation, and the hammering effect of large 1Cr18 particles was localized. In the tamped regions, the particles suffered severe deformation, and the pores were forced to close. The coating remained porous in the nontamped regions. However, at high temperatures (700 °C and 750 °C), the particles were severely deformed because of a higher velocity, and the spherical particles were rarely observed throughout its cross-section. Moreover, the trace of shot-peening particles turned indecipherable.

Fig. 5 shows the porosity levels of TC4 coatings deposited on TC4 substrates at different temperatures based on the image analyses using ImageJ software. Owing to the special structure formed in the *in-situ* shot-peening condition, the porosity was divided into two categories: (i) the regions tamped by shot-peening particles and (ii) those far away from these regions. Although both the results showed a decreasing tendency as a function of accelerating gas temperature, a large gap existed between them. The largest difference is that the values of nontamped regions had a large variation from 15.25% to 4.67%, while those of tamped regions moderately changed from 0.72% to 0.23% as a function of temperature, as well as the standard deviation. The decrease in porosity stems from two reasons: First, It was reported that the highest particle velocities at impact could be achieved at the highest temperatures [26], and particle deformation increased with the increase in impact velocity. Therefore, more deformation occurred in the particles with a higher velocity when compacted to the substrate, leading to a strong decrease in the coating porosity. Thus, clear pores were rarely observed, and the microstructure became dense. Second, regarding the regions nearby the shot-peening craters, the kinetic energy of larger peening particles was probably mainly absorbed by the TC4 particles and converted into plastic deformation. Thus, the original pores were closed, and the porosity sharply decreased. Compared with nontamped regions, it was almost constant with the change in temperature.

In addition, although the feedstock had 70 vol% content of large shot-peening particles, severe erosion did not occur, and the deposition efficiency increased from 64.1% (550 °C) to 74.8% (750 °C) with the increase in temperature, consistent with those reported in literature [27,28].

3.2.2. Local mechanical performance

Fig. 6 shows the Vickers microhardness of TC4 coatings deposited under different accelerating gas temperatures. Because of the special microstructure of coating prepared by *in-situ* shot-peening-assisted cold spraying, the microhardness can also be divided into

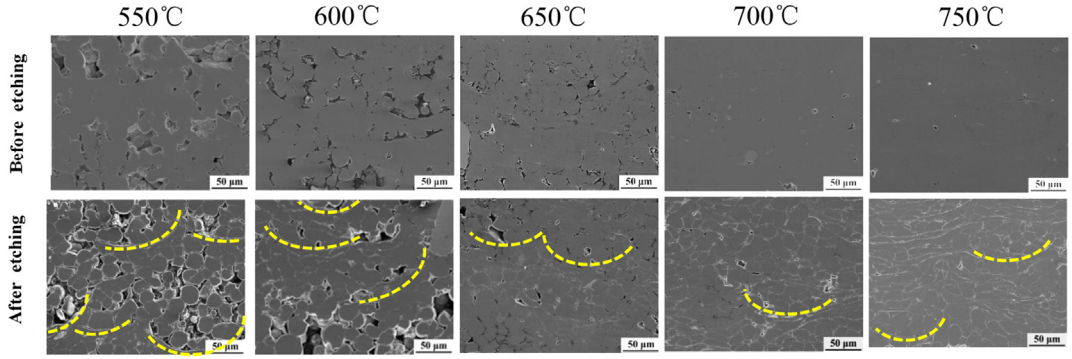

Fig. 4. Cross section morphology of TC4 coatings deposited at different gas temperature using *in-situ* shot-peening assisted cold spraying technology.

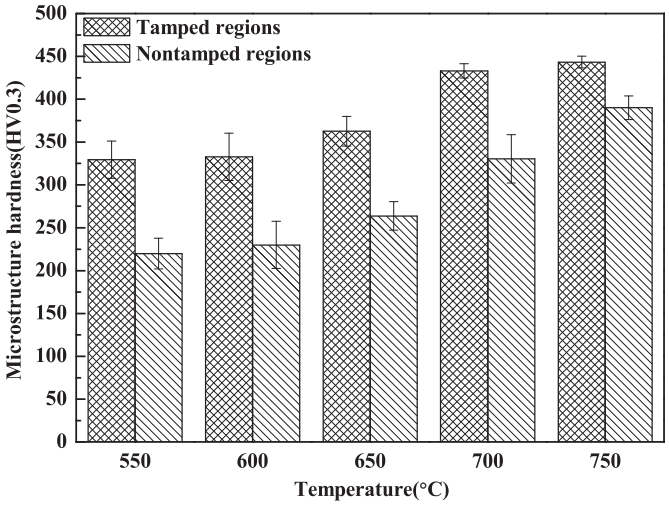

Fig. 6. Vickers microhardness of TC4 coatings as a function of the accelerating gas temperature.

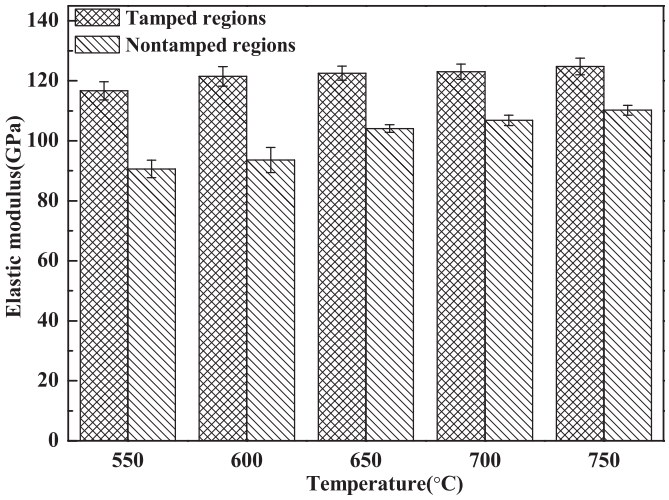

Fig. 7. Elastic modulus of TC4 coatings as a function of the accelerating gas temperature.

two tiers, and the values in regions in/nearby the craters of shot-peening particles were higher than those away from them. The degree of difference in two tiers became smaller with increasing temperature, as well as the standard deviation. Notably, the coating microhardness of both tiers gradually increased with temperature, and the highest hardness was 443.4 $HV_{0.3}$ deposited at 750 °C. The increase in hardness can be attributed to work hardening and decreasing porosity. It was reported that the impact of shot-peening particles induced more shear bands consisting of refined grains or nanograins [29], these refined grains can reduce the dislocation mobility and slipping, and increase the hardness. Furthermore, the difference between the two tiers became smaller, indirectly indicating that the shot effect is weakened at a high temperature. For the coatings prepared at 550 °C and 600 °C, the morphologies of hardness indentations were significantly affected by the pores, and the indentation edge collapsed when the pressure head acted on the surface. Therefore, the coatings prepared at a low temperature had a larger deviation. Consequently, the lower hardness can be mainly attributed to a relatively high porosity. Nevertheless, when the propelling gas temperature was increased to 750 °C, due to the elimination of porosity, the hardness indentation showed an intact quadrilateral surface, and the hardness reached the maximum.

Fig. 7 shows the elastic modulus of TC4 coatings deposited at different accelerating gas temperatures. The elastic modulus of cold-sprayed coatings is a strong indicator of the extent of inter-splat cracking in cold-sprayed coating and thus the quality of coating [30]. As shown in Fig. 7, it can also be divided two categories and has a similar trend as microhardness. As the gas temperature increased from 550 °C to 750 °C, the elastic modulus of tamped regions increased from 116.7 GPa to 124.8 GPa, and that of non-tamped regions increased from 90.6 GPa to 110.2 GPa. At high temperature, the difference of these two categories grew smaller. The increase in elastic modulus can be mainly attributed to a decrease in the porosity of coatings. The porosity in tamped regions is much lower than nontamped regions; therefore, the elastic modulus in tamped regions is higher. In general, the elastic modulus of materials can be measured by three techniques: four-point bending, knoop indentation, and nanoindentation. It is necessary to mention here that the bulk bending of test samples requires a large quantity of particles and interfaces; therefore, the modulus is sensitive to defects such as porosity. In the case of nanoindentation, individual particles are sampled; therefore, the measured elastic modulus is close to the bulk value because of the effect of oxides, and the porosity is reduced [31]. For this reason, there is less difference between the values nearby the shot-peening craters and away from them.

3.3. Tensile and shear properties

Fig. 8 shows the bonding strength of five coatings. With the increase in gas temperature, the bonding strength showed an increasing trend. The bonding strength was 26.6 MPa when the gas inlet temperature was 550 °C, about two times of that of coating prepared at 520 °C, 2.8 MPa, and using air as the propellant gas [32]. The bonding strength of coating prepared at 600 °C reached over 30 MPa, about 10 MPa higher than the coating prepared in a similar situation [33]. When the propelling gas temperature was increased to 750 °C, the bonding strength of coating reached 36.5 MPa, 88% of that of coating prepared at 950 °C, 5 MPa, and with nitrogen as the accelerating gas [9]. It's worth mentioning that one of the testing sample of 750 °C has reached 46.4 MPa. Pelletier [34] summarized the best results in previous reports, and the bonding strength of coating was ~41 ± 4 MPa prepared using helium gas. In contrast, the

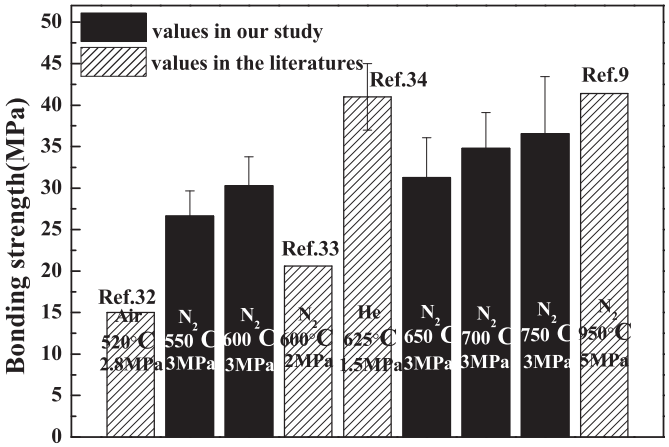

Fig. 8. Bonding strength of TC4 coatings as a function of the accelerating gas temperature.

in-situ shot-peening effect of large stainless steel particles played a great role in enhancing the adhesive strength between coating and substrate. By enhancing the particle deformation, the adhesion of coating and substrate is strengthened. Further, the increase in bonding strength can also be demonstrated from the microstructure of bonding interface, as shown in Fig. 9. More microvoids and continuous microcracks were observed along the coating/substrate interface at 550 °C and 600 °C as shown in the red boxes, indicating that mechanical anchorage will be less under this circumstance. This can be attributed to the combination of a harder substrate material and lower gas temperature, hindering particle deformation and thus resulting in a lower adhesive strength. With the increase in gas temperature, the deformation of particles became greater. Therefore, the interface gap became fuzzy, and deformed particles covered the interface of substrate and coating. Thus, the bonding strength of coating improved.

To further analyze the interface combination status, the fracture interface morphology on the side of coating was shown in Fig. 10. In general, more fracture occurred between the particles, indicating that the adhesion between coating and substrate is stronger than the cohesive between particles. The coating prepared at a lower gas temperature (550–650 °C) are porous, as shown in the amplifying microstructure. The particles still maintained a round shape, and the pores existing between particles slightly deformed. In addition, it can be observed that the crack propagation occurred along the interfaces of particles (as indicated by the yellow arrows in these coatings), and it is speculated that its cohesion strength is mainly determined by the mechanical interlocking strength between the deformed particles. Although for most conditions, the global coating fracture surface was brittle, local ductile regions populated with dimples were present on the fracture surface (as red imaginary circle showed in 650°C coating). With the increase in temperature (700 and 750 °C), the deformation of particles grew severer, and the coating became denser. Pores were rarely observed in the interparticle fracture surface, this is consistent with the results described above. For the higher velocity under high temperature, the narrow interfacial region of the particle experienced intensive deformation, and these regions of high strain were extruded in a plasticized state to form shear lips (as indicated by the yellow arrows in 700 °C and 750 °C coatings), as a result of adiabatic shear instability [35]. Near the edge of combined particles, groups of twins were found, resulting from intensive deformation (as the red arrow showed in 700°Ccoatings). On the interparticle fracture surface, it can be also observed some dimples (the red arrows in 750°Ccoatings), which demonstrated once again that mechanical bonding and metallurgical bonding exist simultaneously in particles cohesion.

Fig. 11 shows that the coating shear strength gradually increased with increasing accelerating gas temperature. As the gas temperature was increased to 750 °C, the shear strength reached 71.18 MPa, triple of that obtained by spraying at 550 °C. The increase in shear strength can be attributed to the gradual decrease in coating porosity and improved particle deformation. Fig. 12 shows the morphology of coating fracture interface. Similar to the structure of fracture interface after tensile strength, the coatings sprayed at a relatively low temperature were porous, and the particles slightly deformed. However, the coatings corresponding to 700 °C and 750 °C exhibited much denser microstructures. The lower porosity and higher deformation of particles confirm that cold spraying parameters, especially accelerating gas temperature, were optimized correctly to achieve a dense material, and the deformation of *in-situ* shot-peening-assisted spray powder and consequent formation of a dense microstructure resulted in a higher performance.

3.4. Coating deposition mechanism

A shot blast is an effective way to improve the densification of Ti alloy cold-sprayed coating. Similar to the above conclusion, the mechanical properties of coatings can be improved in this manner. Because of the particle nature of spraying powder in *in-situ* shot-peening-assisted cold spraying, the coating deposition should be different from single powder. The shot particles significantly affect the coating preparation. Table 2 shows the flattening ratio and action depth of shot at different temperatures. A flattening ratio is defined as the ratio of larger dimension of the splats over the diameter of a circle of equivalent area which was calculated from the splat [36]. By measuring fifty particles, the values were obtained. Because of a large difference in the flattening ratio, depending on the regions where the shot-peening particles tamped or not, the values were divided into two categories. Table 2 shows that the flattening ratio increased on the whole with the increase in temperature. This is because much severe deformation occurred at a higher temperature. In addition, the values in tamped regions were about twenty times larger than nontamped regions. On the other hand, same pores formed at the bottom of craters shown as yellow arrows in Fig. 13. The pores probably formed as a result of the grinding of sample. To determine the reason for pore formation, the behavior of particle deposition in the crater was analyzed. As shown in Fig. 13b, since the crater is cambered, the deposition angle of coming particles always deviates from 90°. According to a correlational study [37], it was not beneficial to the bonding when the sprayed angle was not 90°. Therefore, the particles deposited with less than 90° were easier to fall off when ground.

The action depth of shot was calculated by measuring the depth of crater left by the rebound shot-peening particles (red lines in Fig. 13a), and the value was averaged from ten 1000 × SEM images. The results show that the depth decreased monotonously with increasing temperature, and they are approximately linear as shown in Fig. 14. The average value was ~30.6 μm, amounting to about one spherical spraying particle (calculated using average particle size). Because the depth decreased at a higher temperature, the tamping effect is weakened with the increase in temperature. This is probably because a high velocity at a high temperature

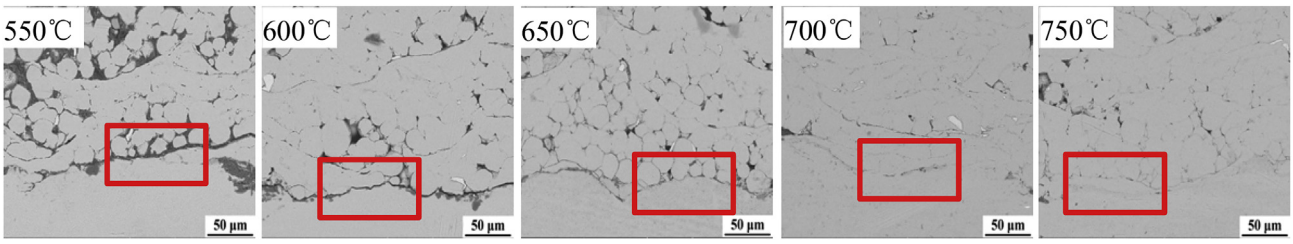

Fig. 9. Bonding interface of TC4 coatings as a function of the accelerating gas temperature.

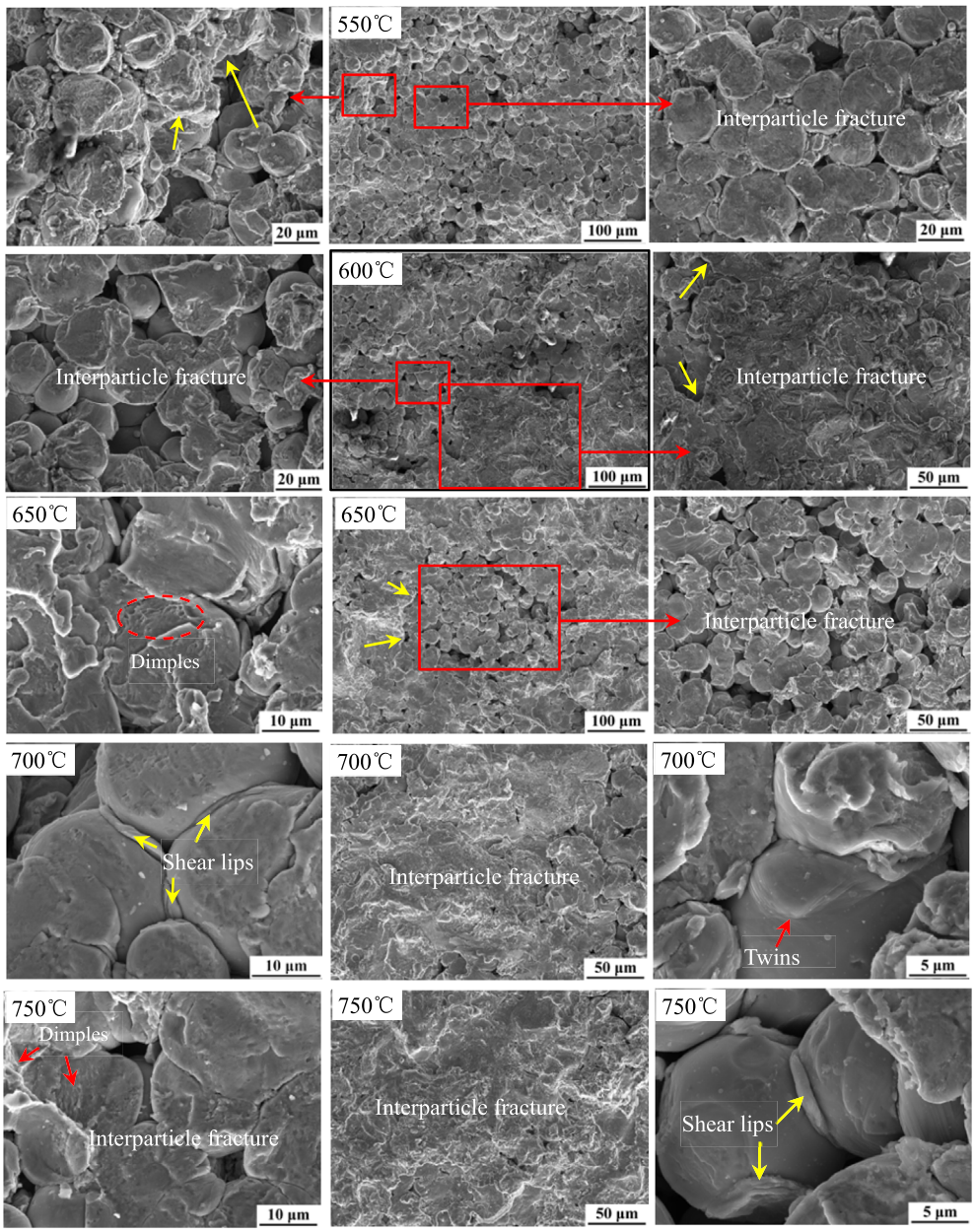

Fig. 10. Fracture morphologies of TC4 coatings.

produced severe TC4 particle deformation accompanied by severe strain strengthening, and the microhardness enhanced as shown in Fig. 6. The strain-strengthening effect reduced the shot-peening effect at a high gas temperature. When the shot-peening particles compacted on much stiffer TC4 deformed particles, it was difficult to make them deform further. The coatings prepared at a high temperature showed a much denser microstructure, and relatively speaking, less pores were present to plug the deformed particles. Although the velocity and kinetic energy of shot-peening particles also increased with the increase in temperature, it seems that the effect of deposit deformation hardening on the action depth of shot is decisive. In other words, *in-situ* shot peening is beneficial to densify TC4 cold-sprayed coating at a relatively low temperature, but the shot effect cannot be enhanced by increasing the gas temperature. The deformation of particle itself at a high temperature is more important for improving the coating property. Fig. 15 showed the top-view surface morphologies of TC4 deposits prepared at 550°Cand 750 °C, the craters induced by shot peening particles can be seen clearly. By contrast, the craters correspond to 550 °C coating are deeper than that of 750 °C, in which the craters are difficult to discern, because of the shallower action depth of the shot peening particles and the overlap between craters. By measuring the diameter of the craters formed in coating of 550 °C, the value ranged from ~140 to ~160 μm was obtained. Taking the average value as 150 μm, the action depth of the shot peening particles can be easily calculated, which is about 40 μm, and this is in good agreement with the statistical result in Table 2.

High-velocity impact studies showed that the crater depth P was linearly related to $(E_p/E_s)\,(\rho_p/\rho_s)^{0.5}$, where E_p and E_s are the elastic moduli of shot-peening particle and substrate, respectively, and ρ_p and ρ_s are the densities [38]. During the *in-situ* shot-peening-assisted cold spraying, the substrate is the deposited coating, and

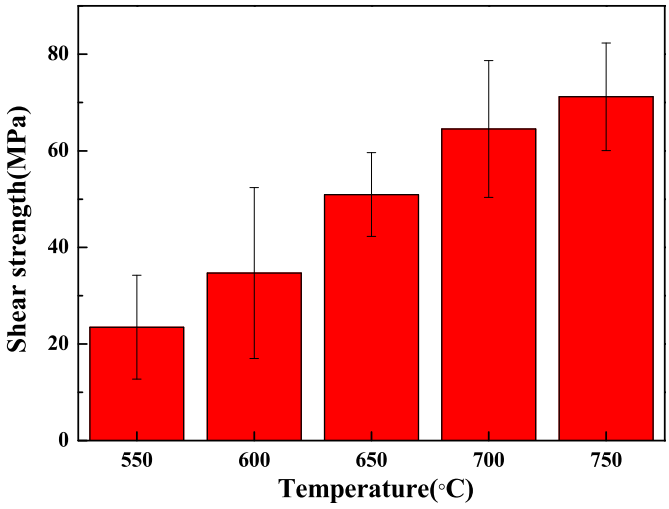

Fig. 11. Shear strength of TC4 coatings as a function of the accelerating gas temperature.

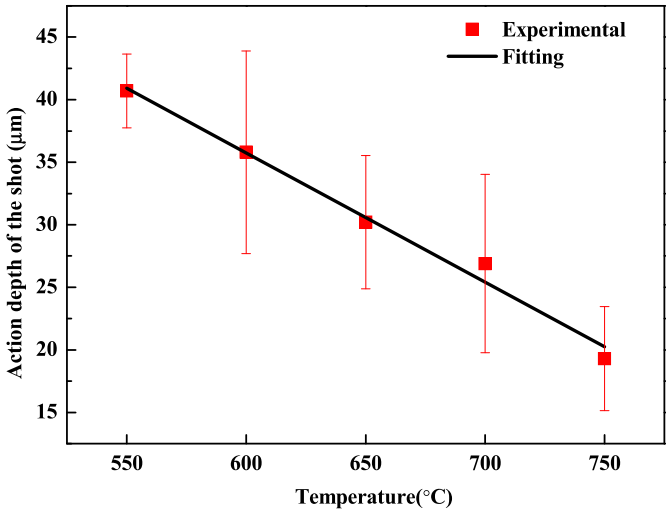

Fig. 14. Action depth of the shot as a function of the accelerating gas temperature.

P is the action depth of shot. Fig. 7 shows that the elastic modulus of coating was increased with increasing temperature and *in-situ* shot-peening effect, indicating that E_s increased. Therefore, according to the relational expression mentioned above, P also decreased. This is consistent with the above observation. Notably, shot-peening particles of large elastic modulus or/and large density can produce a higher P, providing a reference to find more

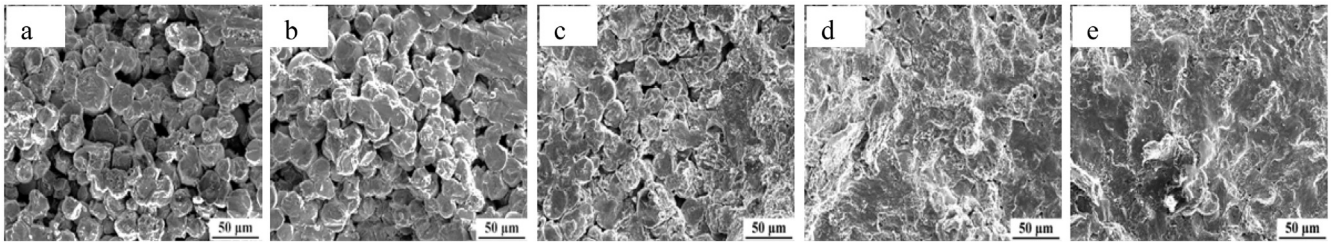

Fig. 12. Fracture interface of TC4 coatings(a) 550 °C,(b) 600 °C,(c) 650 °C,(d) 700 °C,(e) 750 °C.

Table 2
Flattening ratio and action depth of the shot at different temperature.

		550 °C	600 °C	650 °C	700 °C	750 °C
Flattening ratio	Nontamped region	0.46	0.49	0.67	0.96	1.02
	Tamped region	10.44	13.09	20.14	23.13	25.52
Action depth of the shot (μm)		40.7	35.8	30.2	26.9	19.3

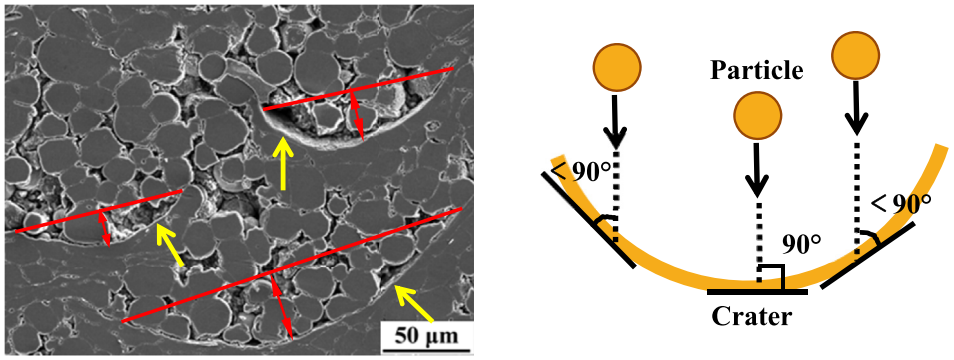

(a) (b)

Fig. 13. Etched microstructure of the 550 °C coating showing how the action depth of the shot is calculated(a) and particle deposition model in crater left by shot peening particle(b).

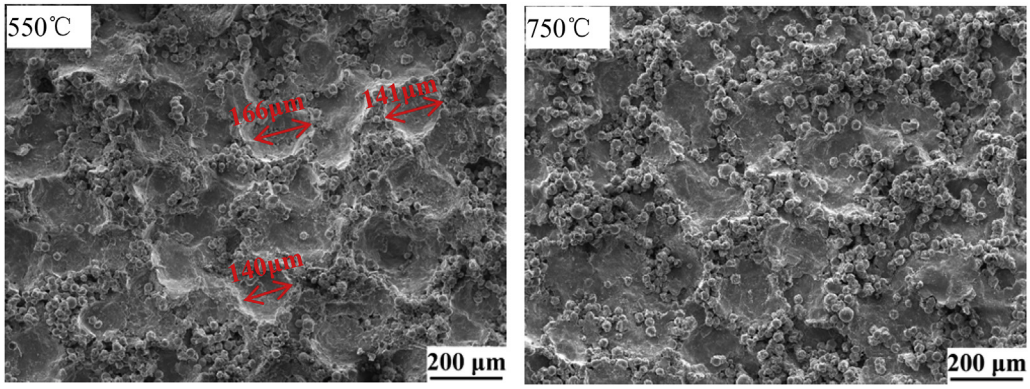

Fig. 15. Surface morphologies of TC4 deposits prepared at 550°Cand 750 °C showing the craters induced by shot peening particles impact.

appropriate shot-peening particles from material selection perspective. Moreover, for the same shot-peening particles, different coating materials can produce different peening effects. This means the coating with a low elastic modulus or/and low density will deform more, and this was confirmed in the study of an Al coating in our group. TC4 has a relatively higher elastic modulus (110 GPa) and higher density (4.5 g/cm^3) than Al (70 GPa and 2.7 g/cm^3, respectively); therefore, the action depth of shot had only two or three particle layers, and the tamped depth was very short.

Fig. 16 shows an illustration of *in-situ* shot-peening-assisted cold-sprayed TC4 coating deposition mechanism. As everyone knows, TC4 is a refractory metal. When it was cold sprayed onto the substrate at a relatively low gas temperature and pressure, the resulting coating had a porous microstructure. The spherical powder maintained the spherical morphology, and pores formed between the particles, as shown in Fig. 4. To eliminate the porosity, the TC4 particles must be deformed. In cold spraying, the deformation of particles significantly depends on velocity. According to Dykhuizen et al. [39], the spraying particle velocity can be expressed as follows:

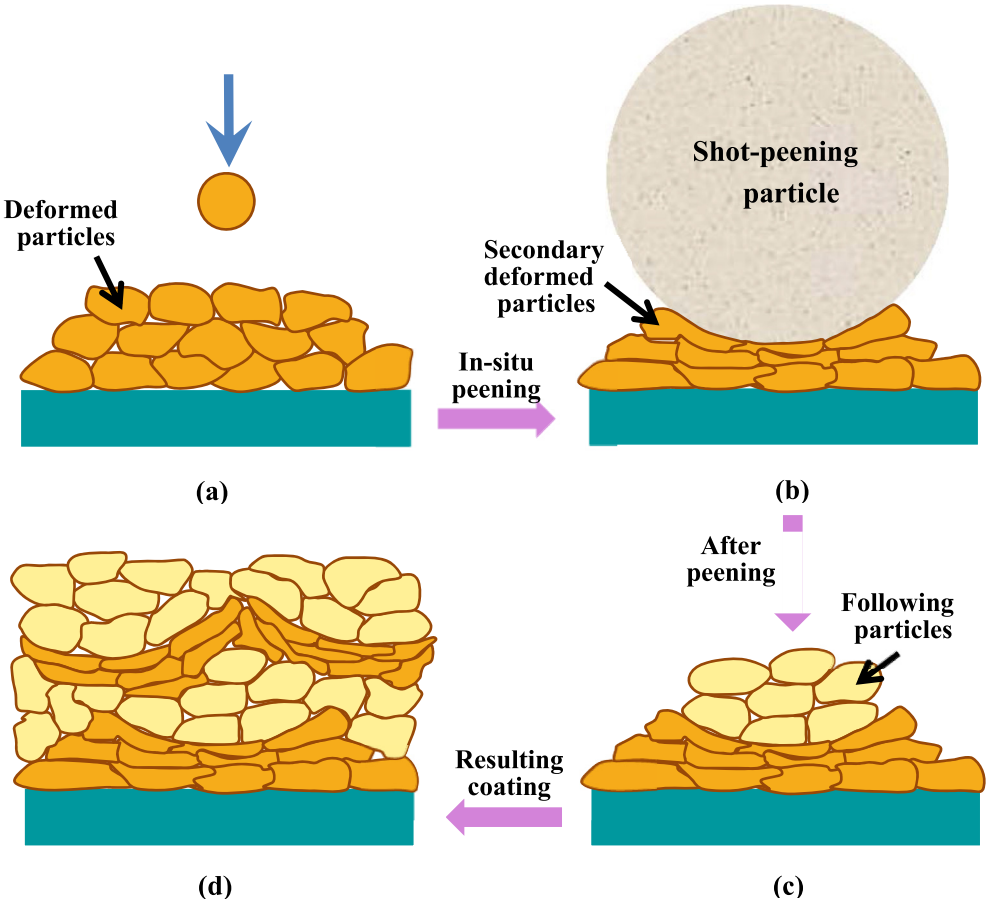

Fig. 16. The illustration of *in-situ* shot-peening assisted cold-sprayed TC4 coating deposition mechanism.

$$V_P = V\sqrt{\frac{C_D A_P \rho x}{m}} \quad (1)$$

$$V = M\sqrt{\gamma RT} \quad (2)$$

where V_p is the particle velocity, V is the gas velocity, C_D is the drag coefficient, A_p is the cross-sectional area of particle, ρ is the gas density, x is the nondimensional axial position, m is the mass of particle, M is the Mach number, γ is the ratio of gas specific heat, T is the gas temperature (K), and R is the specific gas constant. Formula (1) shows that the particle velocity is closely related to the gas velocity: the higher the gas velocity, the higher the particle velocity. However, the gas velocity strongly depends on gas temperature according to Formula (2). Thus, the particle velocity is determined by gas temperature. If the inlet gas temperature increases, the gas velocity as well as particle velocity also increase, increasing the particle deformation (the spherical particle will be deformed into irregular shapes as shown in Fig. 16a). When small TC4 particles are mixed with large 1Cr18 shot-peening particles, constituting a mixed feedstock, the TC4 particles will be deposited when the velocity is higher than the critical velocity, whereas the large shot-peening particles will rebound because the critical velocity of large 1Cr18 particles is much higher than small TC4 particles. Thus, the large 1Cr18 particles with a certain velocity will hammer previous TC4 deposits and make the deformed particles suffer secondary deformation as shown in Fig. 16b. Statistically, the flattening ratio of particles tamped by the shot is about twenty times than that of nontamped particles (Table 2). Large shot-peening particles tend to rebound quickly, and the following TC4 particles keep on depositing. The resulting microstructure exhibits two parts: the top region where the shot tamped is similar to that before the tamping, whereas the regions tamped by shot-peening particles experience abnormal deformation as shown in Fig. 16c. In this manner, by hammering, deforming, and rebounding cycles, a microstructure with an alternating dense and porous structure was formed as shown in Fig. 16d. This microstructure had different local properties such as porosity, microhardness, and elastic modulus. Additionally, because of the auxiliary deformation of shot-peening particles, the macroscopical bonding and shear strengths of the special coating microstructure were enhanced.

4. Conclusions

In this study, TC4 coatings were prepared using an *in-situ* shot-peening-assisted cold spraying technology, and the mechanical properties of the coatings and effect of gas temperature effect were evaluated. The main conclusions drawn from this study are as follows:

- As the temperature was increased from 550 °C to 750 °C, the TC4 coating showed a denser microstructure. Owing to the shot-peening effect, the coating structure showed the characteristics of regionalization: near the regions tamped by shot-peening particles, the coating is denser than nontamped regions. The porosity, microhardness, and elastic modulus can be divided into two categories, and the values of both categories gradually decreased (porosity) or increased (microhardness and elastic modulus) with the increase in temperature. On the other hand, the gap between the two categories narrowed as the temperature increased.
- Because of a high temperature and *in-situ* shot peening, the macroproperties such as bonding and shear strengths reached their maximum at 36.5 MPa and 71.18 MPa, respectively. Moreover, the morphology of fracture surface showed that brittle fracture was the main type of failure.
- By further analyzing the microstructure of coating, it was found the flattening ratio in tamped and nontamped regions varied significantly, but increased on the whole with the increase in gas temperature. However, the action depth of shot had the opposite trend. This indicates that *in-situ* shot peening is beneficial for deforming TC4 particles at a relatively low temperature, but at a high gas temperature, the auxiliary effect of shot peening on the deformation of particles is limited.

Acknowledgements

The authors would like to thank the financial support by the National Science Fund of China (No.51761145108).

Appendix A. Supplementary data

Supplementary data related to this article can be found at https://doi.org/10.1016/j.jallcom.2018.07.009.

References

[1] M. Peters, J. Kumpfert, C.H. Ward, et al., Titanium alloys for aerospace applications, Adv. Eng. Mater. 5 (6) (2010) 419–427.
[2] G. Lutjering, J.C. Williams, Titanium, Springer-Verlag, Berlin, Heidelberg, Germany, 2003, pp. 57–66.
[3] M. Fukumoto, H. Wada, K. Tanabe, et al., Effect of substrate temperature on deposition behavior of copper particles on substrate surfaces in the cold spray process, J. Therm. Spray Technol. 16 (5) (2007) 643–650.
[4] P. Jakupi, P.G. Keech, I. Barker, et al., Characterization of commercially cold sprayed copper coatings and determination of the effects of impacting copper powder velocities, J. Nucl. Mater. 466 (2015) 1–11.
[5] W.Y. Li, H. Liao, C.J. Li, et al., Numerical simulation of deformation behavior of Al particles impacting on Al substrate and effect of surface oxide films on interfacial bonding in cold spraying, Appl. Surf. Sci. 253 (253) (2007) 5084–5091.
[6] T. Wojdat, M. Winnicki, M. Rutkowska-Gorczyca, et al., Soldering aluminium to copper with the use of interlayers deposited by cold spraying, Arch. Civil Mech. Eng. 16 (4) (2016) 835–844.
[7] C.J. Li, W.Y. Li, Y.Y. Wang, Formation of metastable phases in cold-sprayed soft metallic deposit, Surf. Coating. Technol. 198 (1–3) (2005) 469–473.
[8] T. Hussain, D.G. Mccartney, P.H. Shipway, et al., Corrosion behavior of cold sprayed titanium coatings and free standing deposits, J. Therm. Spray Technol. 20 (1) (2011) 260–274.
[9] N.W. Khun, A.W.Y. Tan, K.J.W. Bi, et al., Effects of working gas on wear and corrosion resistances of cold sprayed Ti-6Al-4V coatings, Surf. Coating. Technol. 302 (2016) 1–12.
[10] S. Kumar, V. Vidyasagar, A. Jyothirmayi, et al., Effect of heat treatment on mechanical properties and corrosion performance of cold-sprayed tantalum coatings, J. Therm. Spray Technol. 25 (4) (2016) 745–756.
[11] R. Singh, K.H. Rauwald, E. Wessel, et al., Effects of substrate roughness and spray-angle on deposition behavior of cold-sprayed Inconel 718, Surf. Coating. Technol. 319 (2017) 249–259.
[12] G.C. Ji, X. Chen, H.T. Wang, et al., Deformation behaviors of cold-sprayed WC-Co particles, J. Therm. Spray Technol. 24 (6) (2015) 1100–1110.
[13] N.W. Khun, A.W.Y. Tan, W. Sun, et al., Effect of heat treatment temperature on microstructure and mechanical and tribological properties of cold sprayed Ti-6Al-4V coatings, Tribol. Trans. (2016) 1–10.
[14] S.H. Zahiri, C.I. Antonio, M. Jahedi, Elimination of porosity in directly fabricated titanium via cold gas dynamic spraying, J. Mater. Process. Technol. 209 (2) (2009) 922–929.
[15] W. Wong, P. Vo, E. Irissou, et al., Effect of particle morphology and size distribution on cold-sprayed pure titanium coatings, J. Therm. Spray Technol. 22 (7) (2013) 1140–1153.
[16] W. Wong, A. Rezaeian, E. Irissou, et al., Cold spray characteristics of commercially pure Ti and Ti-6Al-4V, Adv. Mater. Res. 89–91 (2010) 639–644.
[17] D. Goldbaum, J.M. Shockley, R.R. Chromik, et al., The effect of deposition conditions on adhesion strength of Ti and Ti6Al4V cold spray splats, J. Therm. Spray Technol. 21 (2) (2012) 288–303.
[18] M.V. Vidaller, A. List, F. Gaertner, et al., Single impact bonding of cold sprayed Ti-6Al-4V powders on different substrates, J. Therm. Spray Technol. 24 (4) (2015) 644–658.
[19] J.L. Pelletier, Development of Ti-6Al-4V Coating onto Ti-6Al-4V Substrate Using Low Pressure Cold Spray and Pulse Gas Dynamic Spray, 2013.
[20] C. Lee, J. Kim, Microstructure of kinetic spray coatings: a review, J. Therm.

Spray Technol. 24 (4) (2015) 592–610.
[21] W.Y. Li, H. Liao, C.J. Li, et al., Numerical simulation of deformation behavior of Al particles impacting on Al substrate and effect of surface oxide films on interfacial bonding in cold spraying, Appl. Surf. Sci. 253 (253) (2007) 5084–5091.
[22] R. Huang, The Importance of Optimizing Nozzle Dimensions for Cold Spray Process[C], 2015.
[23] C.J. Li, W.Y. Li, Deposition characteristics of titanium coating in cold spraying, Surf. Coating. Technol. 167 (2–3) (2003) 278–283.
[24] X.T. Luo, Y.K. Wei, Y. Wang, et al., Microstructure and mechanical property of Ti and Ti6Al4V prepared by an in-situ shot peening assisted cold spraying, Mater. Des. 85 (2015) 527–533.
[25] G. Bae, K. Kang, J.J. Kim, et al., Nanostructure formation and its effects on the mechanical properties of kinetic sprayed titanium coating, Mater. Sci. Eng. A 527 (23) (2010) 6313–6319.
[26] R.C. Dykhuizen, M.F. Smith, Gas dynamic principles of cold spray, J. Therm. Spray Technol. 7 (2) (1998) 205–212.
[27] W.Y. Li, C. Zhang, X. Guo, et al., Ti and Ti-6Al-4V coatings by cold spraying and microstructure modification by heat treatment, Adv. Eng. Mater. 9 (5) (2007) 418–423.
[28] G. Bae, S. Kumar, S. Yoon, et al., Bonding features and associated mechanisms in kinetic sprayed titanium coatings, Acta Mater. 57 (19) (2009) 5654–5666.
[29] D. Goldbaum, R.R. Chromik, N. Brodusch, R. Gauvin, Microstructure and mechanical properties of Ti cold-spray splats determined by electron channeling contrast imaging and nanoindentation mapping, Microsc. Microanal. 21 (3) (2015) 570–581.
[30] G. Sundararajan, N.M. Chavan, S. Kumar, The elastic modulus of cold spray coatings: influence of inter-splat boundary cracking, J. Therm. Spray Technol. 22 (8) (2013) 1348–1357.
[31] T. Hussain, Cold spraying of titanium: a review of bonding mechanisms, microstructure and properties, Key Eng. Mater. 533 (53) (2012) 53–90.
[32] W.Y. Li, C. Zhang, X. Guo, et al., Ti and Ti-6Al-4V coatings by cold spraying and microstructure modification by heat treatment, Adv. Eng. Mater. 9 (5) (2007) 418–423.
[33] L. JIN, X.Z. Cui, Y.F. Ding, et al., Critical deposition velocity calculations and properties investigations of TC4 cold spray coatings, Surf. Technol. 46 (8) (2017) 96–101 (In Chinese).
[34] J.L. Pelletier, Development of Ti-6Al-4V Coating onto Ti-6Al-4V Substrate Using Low Pressure Cold Spray and Pulse Gas Dynamic Spray, 2013.
[35] Assadi Hamid, Gärtner Frank, Thorsten Stoltenhoff, et al., Bonding mechanism in cold gas spraying, Acta Mater. 51 (15) (2003) 4379–4394.
[36] G. Sundararajan, N.M. Chavan, S. Kumar, The elastic modulus of cold spray coatings: influence of inter-splat boundary cracking, J. Therm. Spray Technol. 22 (8) (2013) 1348–1357.
[37] S. Yin, X. Suo, J. Su, et al., Effects of substrate hardness and spray angle on the deposition behavior of cold-sprayed Ti particles, J. Therm. Spray Technol. 23 (1) (2014) 76–83.
[38] L.E. Murr, S.A. Quinones, E.T. Ferreyra, A. Ayala, O.L. Valerio, F. Hörz, R.P. Bernhard, The low-velocity-to-hypervelocity penetration transition for impact craters in metal targets, Mater. Sci. Eng. A 256 (1998) 166–182.
[39] R.C. Dykhuizen, M.F. Smith, Gas dynamic principles of cold spray, J. Therm. Spray Technol. 7 (2) (1998) 205–212.